Journal of Thermal Analysis and Calorimetry (2020) 141:1207–1219
https://doi.org/10.1007/s10973-019-09112-9

Experimental and numerical study of natural convection in bottom-heated cylindrical cavity filled with molten salt nanofluids

Qiang Yu[1] · Yuanwei Lu[1] · Cancan Zhang[1] · Yuting Wu[1] · Bengt Sunden[2]

Received: 23 September 2019 / Accepted: 26 November 2019 / Published online: 18 December 2019

Abstract
This paper combines numerical and experimental to study the heat transfer by free convection for nanofluids of molten salt within a cavity with cylindrical shape which is heated at the bottom and releases heat at the top. The aim is to acquire the free convection laws for nanofluids of molten salt in a cylindrical cavity. It is found that after adding nanoparticles, the molten salts have lower viscosity, higher flow velocity and higher heat transfer rate, and therefore, the free convection heat transfer is enhanced. Meanwhile, nanofluids Nusselt number is larger than that of the molten salts at the same Rayleigh number. In addition, as the classical Garon's equation cannot provide good predictions of free convection heat transfer for the nanofluids of molten salt, this paper establishes a free convection equation for the nanofluids of molten salt in a cylindrical cavity. This equation is able to predict with an error less than 20% the experimental results. Therefore, the findings can provide a basis for engineering applications of nanofluids and for designing optimal systems of heat stockpile with a single tank.

Keywords Cylindrical cavity · Molten salts · Nanofluids · Natural convection

List of symbols

Nu	Nusselt number
Ra	Rayleigh number
Pr	Prandtl number
d	Diameter of cavity (m)
I	Electric current (A)
U	Voltage (V)
Q_T	Total heating power of heater (W)
Q_R	Radiative heat dissipation per unit time (W)
Q	Heat flux of natural convection (W)
A	Heating area (m^2)
h	Heat transfer coefficient (W m^{-2} K^{-1})
T_{wo}	Surface temperature of external wall of thermal insulation layer (K)
T_a	Ambient temperature (K)
T_w	Bottom temperature (K)
ΔT	Temperature difference between bottom and top surface (K)
l	Distance between bottom and top surface (m)
T_c	Top temperature (K)
T_m	Average temperature (K)
T	Temperature (K)
ρ	Density (kg m^{-3})
λ	Thermal conductivity (W m^{-1} K^{-1})
T_c	Top temperature (K)
T_f	Qualitative temperature (K)
ρ_c	Density at T_c temperature (kg m^{-3})
g	Acceleration caused by gravity (m s^{-2})
ρ_f	Density of base salt (kg m^{-3})
ρ_{nf}	Density of nanofluid (kg m^{-3})
$(C_p)_f$	Specific heat of base salt (J kg^{-1} K^{-1})
$(C_p)_{nf}$	Specific heat of nanofluid (J kg^{-1} K^{-1})
μ_f	Viscosity of base salt (Pa S)
μ_{nf}	Viscosity of nanofluid (Pa S)
λ_f	Thermal conductivity of base salt (W m^{-1} K^{-1})
λ_{nf}	Thermal conductivity of nanofluid (W m^{-1} K^{-1})
v_f	Velocity of base salt (m s^{-1})
v_{nf}	Velocity of nanofluid (m s^{-1})

Greek letters

ε	Surface emissivity $\varepsilon = 0.05$
σ_b	Blackbody radiation constant $\sigma_b = 5.67 \times 10^{-8}$ (W m^{-2} K^{-4})
ν	Kinematic viscosity (m^2 s^{-1})

✉ Yuanwei Lu
luyuanwei@bjut.edu.cn

[1] Key Laboratory of Enhanced Heat Transfer and Energy Conservation, Ministry of Education of China, College of Environmental and Energy Engineering, Beijing University of Technology, Beijing 100124, China

[2] Department of Energy Sciences, Lund University, P.O. Box 118, 22100 Lund, Sweden

α Thermal diffusivity($m^2\ s^{-1}$)
β Coefficient of thermal volume expansion (K^{-1})

Introduction

Over the last several years, concentrating solar power (CSP) technologies have been considered as the most promising approach for generating renewable electric power because they can be combined with the low-cost and widely used thermal energy storage technologies to respond to issues such as energy shortage and environmental pollution [1–3]. The design of heat storage-release systems and the selection of heat storage-release materials are the key technologies for concentrating solar power.

Dual-tank system of energy store is now most extensively applied within CSP demonstration plants, but its cost is too high. To cut down the cost, the system of fusional salt heat stockpile with single jar is put forward by our team. In this system, the submerged-pipe coil heat-exchange facility is arranged for single-tank storage and release of thermal energy [4]. The molten saltside heat transfer is natural convection during the single-tank energy storage and release processes, so heat transfer must be carefully considered in designing the system of fusional salt heat stockpile with a single tank.

Molten salt can make CSP technologies more efficient and reliable as a thermal fluid. In addition, applying fusional salt as the heat carrying agent can realize low-cost and large-scale energy storage and ensure the output of high-quality electric power through CSP technologies. Therefore, the use of this fluid as a heat transfer carried has become central to the development of CSP technologies. However, as molten salt has a low thermal conductivity and a low specific heat, its heat transfer and storage properties are severely limited. To improve these two properties, an effective way is to add nanoparticles into the molten salt. Nanofluid technologies can enhance the heat transfer capacities of fluids, thereby making the thermal energy storage system more efficient.

Convective heat transfer of nanofluids has been extensively studied over the last several years. In numeral simulations, Ahmed [5] used the finite difference method to study two-dimensional steady-state laminar MHD mixed convection flow in a square inclined cavity. It was found that the nanofluid was better than water to enhance the heat transfer when the effect of the magnetic field was weak, while water was better than the nanofluid when the magnetic effect was strong. Shirazi [6] studied mixed convection heat transfer of water–Al_2O_3 nanofluids between two cylinders. The results showed that within the entire range of Rayleigh number $10^3 \leq Ra \leq 10^5$ and Richardson number $0.1 \leq Ri \leq 100$, an increase in Rayleigh and Richardson numbers leads to an increase in the average Nusselt number on the inner cylinder wall. Rashmi [7] utilized the Fluent software to study Al_2O_3 nanofluids based on water for free convection within a horizontal cylindrical cavity. It was discovered that the convective heat transfer diminished with the increase in nanoparticles volume fraction. Oztop [8] studied natural convection heat transfer at steady state within chambers filled with two distinct nanoparticles, namely Al_2O_3 and TiO_2. He discovered that nanoparticles addition would affect the fluid flow and temperature distributions, especially when the *Ra* number was high. Mahmoodi [9] researched free convection heat transfer and flow of nanofluids based on water. The right and left walls of the rectangular cavity were kept at constant temperatures, while the lower and upper walls were heat retaining. The heater was situated inside this cavity. The results showed that the rate of heat transfer increased as the *Ra* number was increased. Lai and Yang [10] studied free convection heat transfer of Al_2O_3 nanofluids based on water under two conditions, namely a constant *Ra* number and a constant temperature difference. It was noted that the average *Nu* number increased with *Ra* number, while the relative *Nu* number increased with the average fluid temperature as well as with the temperature difference between the side walls. Sokhansefat [11] carried out a simulation study on the heat transfer utilizing a nanofluid of Al_2O_3/synthetic oil within an unevenly heated parabolic collector tube. The author found that the convective heat transfer coefficient increased as the nanoparticles volume fraction increased, while it decreased when the temperature increased. Mwesigye [12, 13] added nanoparticles into synthetic oil with the aim to study oil heat transfer properties. The author found that nanoparticle addition at a temperature between 77 and 327 °C could enhance the efficiency of the receiver by 8–13%.

As it is difficult to prepare nanofluids and to measure their properties, the experimental researches of nanofluids within a closed cavity under free convection are very limited. Putra [14] carried out experiments on nanofluids with CuO and Al_2O_3 particles based on water under free convection within a horizontal cylindrical cavity. It was discovered that the nanoparticles presence deteriorated natural convection heat transfer, which was thought to be the possible result of aggregation and sedimentation of the nanoparticles. Suhaib [15] used an experimental method to study natural convection heat transfer characteristics in a vertical rectangular enclosure. The results showed that the cooling performance of MWCNT-hot oil-based nanofluids is adversely affected in natural convection heat transfer, despite that high thermal conductivity is observed in nanofluids. Subramanian [16] studied heat transfer of TiO_2–water nanofluids in a heat exchanger. The results showed that the heat transfer of nanofluids is higher than that of the base fluid (water), and increased with increasing Reynolds number. Torki [17] studied natural convection heat transfer of nano-SiO_2/water in a rectangular enclosure with different concentrations and

inclinations. It was found that the effect of nanofluid concentration on Nusselt number decreased with increased cavity inclination. Ming and Pan [18] researched the influence of nanoparticles on fusional salt heat transfer properties in a round tube. It was revealed that when nanoparticles of Al_2O_3 were added to the fusional salt with concentrations from 0.016 to 0.25%, the average *Nu* number increased by 6.9–11.6%. For all molten salt-based nanofluids, the average *Nu* numbers became higher due to the added Al_2O_3 nanoparticles (Table 1).

As indicated by the foregoing discussion, most results show that the nanofluids obviously increase the traditional fluids heat transfer capacity. However, the results of experiments show that nanoparticles presence may worsen the heat transfer. There are more researches on free convection heat transfer of nanofluids based on water and less reports on free convection heat transfer of fusional salts. In this paper, nanofluids of fusional salt under free convection heat transfer within a cylindrical cavity are studied by numerical calculation and experiments. The results can provide a basis for engineering applications of nanofluids and for designing optimal systems of heat stockpile with a single jar.

Numerical calculation of natural convection heat transfer in nanofluids

Computational domain and boundary conditions

The assumptions of heat transfer along with flow are simplified before establishing free convection pattern:

1. The fluid is an incompressible Newtonian fluid, and the flow in the cavity is three dimensional.
2. The viscous dissipation heat is negligible.
3. In the calculation process, the wall of the cylindrical cavity is insulated, so the heat loss of the wall is not considered.

A cylindrical cavity is used as the physical model for the numerical calculations. The cylindrical cavity has a diameter of 150 mm and a height of 140 mm. To keep accuracy of the study, the structure of the cylindrical cavity is simplified. Because the calculation domain is symmetrical, half of this region is in the simulations, as shown by the colored half of the cylinder in Fig. 1. The Ansys CFX software is applied for the numerical simulations of free convection for the nanofluids of fusional salt in the cylindrical cavity. A

Table 1 Summary of experimental and numerical studies on the natural convection heat transfer of nanofluids

References	Experimental and numerical	Particle material	Base fluid	Parameters
Ahmed [5]	Numerical	Cu	Water	$0° \le \varphi \le 175°$
Shirazi [6]	Numerical	Al_2O_3	Water	$10^3 \le Ra \le 10^5$ $0.1 \le Ri \le 100$
Rashmi [7]	Numerical	Al_2O_3	Water	$\varphi \le 1\%, 4\%$ $A = 1.0$
Oztop [8]	Numerical	Al_2O_3/TiO_2	Water	$10^3 \le Ra \le 10^5$ $0 \le \varphi \le 10\%$ $A = 1.0$
Mahmoodi [9]	Numerical	$Cu/TiO_2/Ag$	Water	$10^3 \le Ra \le 10^6$ $0 \le \varphi \le 9\%$ $A = 1.0$
Yang [10]	Numerical	Al_2O_3	Water	$10^3 \le Ra \le 10^6$ $0 \le \varphi \le 4\%$ $A = 1.0$
Sokhansefat [11]	Numerical	Al_2O_3	Synthetic oil	
Mwesigye [12, 13]	Numerical	Al_2O_3/TiO_2	Synthetic oil	$3.5 \times 10^3 \le Ra \le 10^6$ $0 \le \varphi \le 8\%$
Putra [14]	Experimental	CuO/Al_2O_3	Water	$10^7 \le Ra \le 10^9$ $\varphi = 1\%, 4\%$ $A = 0.5, 1.0$
Suhaib [15]	Experimental	MWCNT	Oil	$415 \le Pr \le 600$
Subramanian [16]	Experimental	TiO_2	Water	$\varphi = 0.1\%, 0.3\%, 0.5\%$ d = 20 nm
Torki [17]	Experimental	SiO_2	Water	$\varphi \le 0.1$ vol% $0° \le \tau \le 120°$
Ming [18]	Experimental	Al_2O_3	Salt	$0.016\% \le \varphi \le 0.25\%$

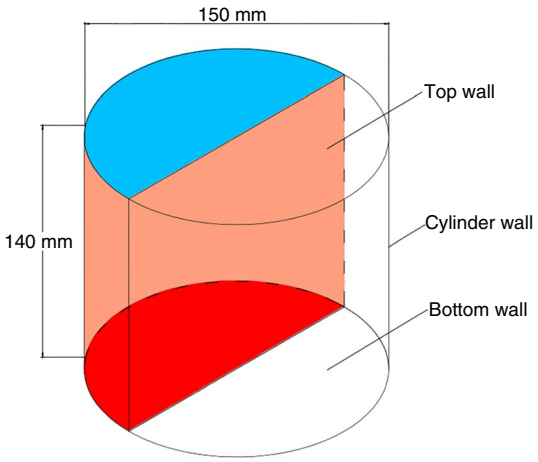

Fig. 1 Schematic diagram of computational domain

three-dimensional unsteady turbulent flow model is applied, and a second-order scheme of upwind differences is used to calculate momentum and energy transport. The convergence criterion is defined, so that the absolute value of the mass residual must be lower than 1×10^{-5} and the energy residual should be lower than 1×10^{-6}. The bottom wall is heated to a high temperature, while the top wall is heated to a low temperature, and the vertical wall of the cylinder is insulated. By controlling the bottom wall temperature, the intensity of the heat flow is changed, and so is the *Ra* number.

Grid independence verification

A finite volume approach is adopted for the mesh generation. Because the number of meshes near the walls at the bottom and the top would affect the simulation results considerably, meshes near these two walls are refined and made denser during the mesh generation. The mesh generation has been introduced in detail in a previous study [19].

In the numerical computations, the mesh quality will affect the accuracy and speed of the computations. In order to ensure the quality of the mesh, water is used as a medium to verify the grid independence. Table 2 reveals the relation between the convective heat transfer coefficient and the number of grids. It can be seen from the table that convective heat transfer coefficient is greatly affected by the number of grids between 50,000 and 60,000. The grids in this range are not suitable for numerical calculations. When the grid number is between 62,000 and 83,000, the convective heat transfer coefficient is less affected by the grid number. Within this study, the number of grid is chosen as 73,953 (3).

Table 2 Grid independence test of water

Number	Grid number	h/W m^{-2} K^{-1}
1	54720	131.68
2	62880	132.29
3	73953	132.29
4	83540	132.31
5	93762	132.36

Experimental equipment and methods of natural convection heat transfer

Experimental system

Figure 2 shows the schematic diagram of the system for experiments of nanofluids at free convection heat transfer. An electric resistance heater was installed on the bottom wall of the cavity, and it was connected to a 220-volt AC supply in a series connection to heat the molten salt nanofluids in the cavity. A sliding rheostat was connected to the circuit in series with the aim to regulate the bottom wall electric resistance heating power. The heating power of the cavity is measured by a voltmeter and an amperometer. The heater had a maximum power of 300 W and was required to withstand a high temperature of 500–600 °C. It was possible to heat evenly so that the temperature variation of the bottom wall was within 1 K. Heat transfer by conduction and convection induced by the heater in this experiment was approximated to be only in the vertical direction.

The cavity in the experiment was made up of a cylindrical cavity, a thermal insulation layer and molten salt nanofluids. The cylindrical cavity was 150 mm in inner diameter and

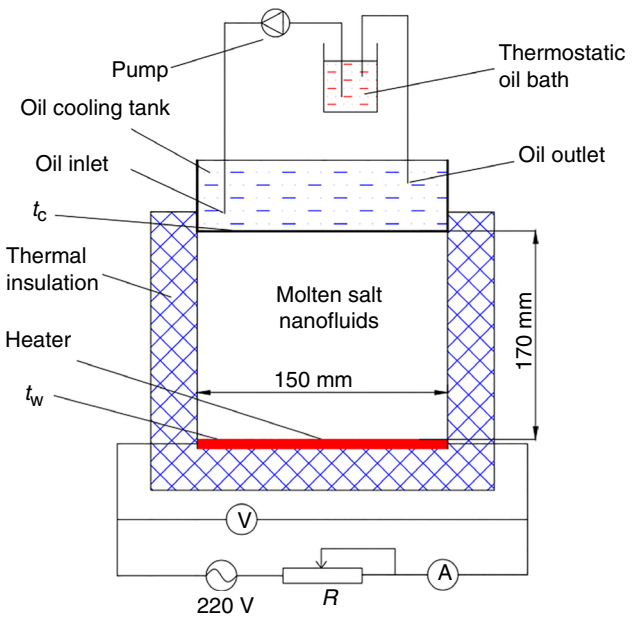

Fig. 2 Natural convection heat transfer experimental setup

170 mm in height. It was covered with a 125 mm-thick layer of thermal insulation material to reduce heat losses to the surroundings. The fusional salt nanofluid in the cavity was 140 mm high after complete melting. An oil cooling tank was installed on the top wall of the cavity to take away the fluid heat. To measure temperature variations at different positions during the natural convection, temperature measurement points were installed on the top and bottom walls as well as in the cavity at various heights inside the experimental setup. Detailed information of the measurement point installations in the cavity is available in [19].

Experimental data analysis

In the free convection experiment, the heating power Q_T is changed via adjusting the current I and voltage U. The bottom area A is obtained by the bottom diameter. The bottom and the top temperatures of the cylinder cavity are measured by thermocouples, and the temperature difference ΔT is acquired. Then, the heat transfer coefficient h can be obtained.

The heating power Q_T is calculated as:

$$Q_T = UI \tag{1}$$

With Stefan–Boltzmann's law, the heat loss to the surroundings is determined as:

$$Q_R = \varepsilon A \sigma_b \left(T_{wo}^4 - T_a^4\right) \tag{2}$$

Then, by applying Eqs. (1) and (2), the heat flux by free convection is found:

$$Q = Q_T - Q_R \tag{3}$$

By Eq. (3), the convective heat transfer coefficient can be calculated as:

$$Nu = \frac{hl}{\lambda} = \frac{ql}{\Delta T \lambda} = \frac{Ql}{\Delta T A \lambda} \tag{4}$$

The Rayleigh number Ra is calculated by Eq. (5):

$$Ra = \frac{\beta g \left(T_w - T_c\right) l^3}{\nu \alpha} \tag{5}$$

The coefficient of volumetric expansion can be estimated by Eq. (6):

$$\beta = \frac{\rho_c - \rho}{\rho \left(T - T_c\right)} \tag{6}$$

The average temperature is determined by Eq. (7):

$$T_m = \left(T_w + T_c\right)/2. \tag{7}$$

Reliability verification of the computational model and experimental system

Before the numerical simulations and experiments of the nanofluids of fusional salt during free convection in the cylindrical cavity, the reliability of the calculation model and experimental setup was studied for water. In the experiment, the applied current began at 0.2 A and then increases by 0.1 A. After steady state was achieved, the relevant data for different heating conditions were recorded. The free convection Nu number of water in the cavity was obtained via experiments and numerical calculations, and comparison with Garon's [20] correlation was carried out, as shown in Fig. 3. It can be seen from the figure that the Nu number of water increases as the Ra number increases in the range of $7 \times 10^7 \leq Ra \leq 1.2 \times 10^9$. The maximum deviation of the results of simulations and experiments from the correlation is less than 10%. Therefore, the established experimental setup and the numerical method are reliable. Based on this, free convection of nanofluids of fusional salt can be studied satisfactorily.

Thermophysical properties of base salt and nanofluids preparation

Thermophysical properties of base salt

Ren [22] developed a new quaternary mixed molten salt, which is used as base salt. The fusional salt fusing point is 96.8 °C, which is about 40 and 130 °C lower than Hitec and Solar Salt fusing point, respectively. The temperature of disintegration is 612.0 °C. Two kinds of experimental studies to achieve thermal stability at large differences in temperature for cool–hot quenching and maintain a certain

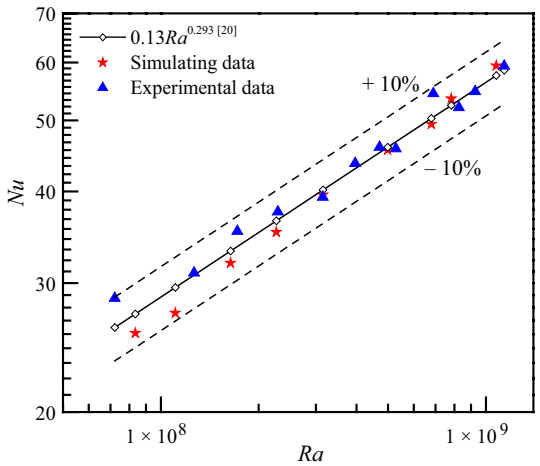

Fig. 3 Natural convection heat transfer of water

high temperature are processed. The experiment at large temperature differences for quenching cool and heat contains 1000 cycles from room temperature to 520 °C. The experiment at a certain high temperature lasts 1200 h at 520 °C. The experimental results fully proved fusional salt thermostability. Ren et al. measured viscosity, thermal conductivity, specific heat as well as density. The specific parameters can be estimated as follows [21, 22].

(1) Density, kg m^{-3}

The density ρ_f of the base salt is a function of temperature:

$$\rho_f = 2038 - 0.5679 \times (T - 273.15) \quad 390\,K \le T \le 773\,K \tag{8}$$

(2) Specific heat, J kg^{-1} K^{-1}

The specific heat $(C_p)_f$ can be estimated as follows.

$$\left(C_p\right)_f = 1450 + 0.3451 \times (T - 273.15) \quad 390\,K \le T \le 773\,K. \tag{9}$$

(3) Viscosity, Pa s

The viscosity μ_f is an important parameter in the natural convective heat transfer process. The viscosity of the mixed salt can be written as follows.

$$\mu_f = 0.007363 \exp\left[-(T - 273.15)/244.509\right] + 0.998 \times 10^{-3} \quad 390\,K \le T \le 773\,K \tag{10}$$

(4) Thermal conductivity, W m^{-1} K^{-1}

The temperature has little effect on the thermal conductivity of the molten salt, which is approximately 0.53 W m^{-1} K^{-1}.

Molten salt nanofluids preparation and its physical properties

Molten salt nanofluids preparation

The preparation methods of nanofluids of fusional salt are as follows.

1. Alkali salt preparation. Base salt is prepared via mixing of four types of nitrates, i.e., KNO_3 and $Ca(NO_3)_2{\cdot}4H_2O$, $LiNO_3$ as well as $NaNO_3$, which have 99.9% purity at a certain ratio of 2:6:1:2.
2. Melting of base salt. The composition of the composite is quaternary mixed molten salt and SiO_2 nanoparticles. The diameter of SiO_2 nanoparticles is 20 nm, and the mass fraction is 1 mass% [23, 24]. The total mass in the experiment is 5 kg, of which the molten salt is 4975 g and SiO_2 nanoparticles is 25 g. The base salt is placed in the cylindrical cavity and is heated to 300 °C with the bottom heater and stirred for half an hour.
3. The preparation of nanofluids. SiO_2 particles of 25 g are added to the fusional base salt slowly and mixed efficiently at the time of mixing for 15 min, and the speed of stirring is 750 rpm [25]. Then, nanoparticles are dispersed uniformly in the base salt and the molten salt nanofluids are obtained.

Molten salt nanofluids stability

The solubility of SiO_2 nanoparticles in water is very low and hydrophobic, but the molten salt is ionic liquid, and the solubility of SiO_2 nanoparticles in molten salt is large. Different researchers [23–26] dispersed different contents of SiO_2 nanoparticles into molten salt. The results showed that when the mass fraction of SiO_2 nanoparticles is 1%, stable nanofluids can be obtained. Zhang [27] prepared molten salt nanocomposites with 1 mass% nanoparticles added. It was found that the addition of nanoparticles had a positive impact on the thermal properties of the base salt. Song [28] studied the thermophysical properties of molten salt nanofluids by a mechanical dispersion method. It was found that the thermophysical properties of the molten salt were greatly improved by adding 1 mass% nanoparticles. Therefore, on the basis of previous studies, we have investigated natural convection heat transfer of nanofluids and adopted the optimal addition ratio recommended. Song [28] found that the specific heat, thermal conductivity and other thermal properties of the molten salt nanocomposites did not change significantly through high-temperature constant temperature and large temperature difference quenching/thermal experiment, which confirmed that the molten salt nanocomposites prepared by mechanical stirring method had good stability.

In order to investigate the distribution of SiO_2 nanoparticles in the base salt, the surface microstructure of the base salt and molten salt nanocomposites is measured by SEM. Figure 4a shows the surface structure of the base salt without adding nanoparticles. It can be seen that the surface of the base salt is relatively flat and smooth. Figure 4b shows the microstructure of the molten salt added 1 mass% SiO_2 nanoparticles. Compared with the base salt, the surface of the molten salt nanocomposites has nearly uniform distribution of small particles, which reduces the surface smoothness and increases the brightness. The structure formed by these

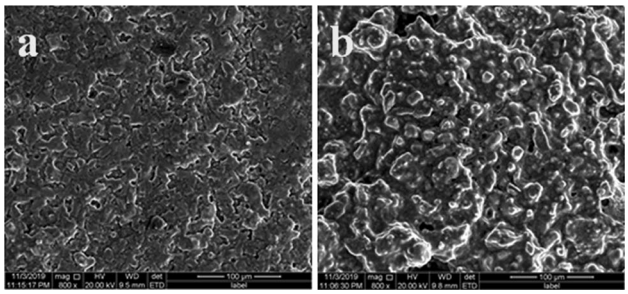

Fig. 4 SEM: **a** Base salt, **b** Molten salt nanocomposites

uniformly distributed particles is called nanostructure, which effectively increases the specific surface area of molten salt.

Moreover, an EDS element mapping measurement was performed to see the distribution of element Na, K, Ca, Si, O, N in the molten salt nanocomposite. The element mapping results are shown in Fig. 5. We can see from the figures that the nanoparticles represented by element Si are uniformly dispersed in the composite. At the same time, a uniform nanostructure can be formed on composite surface and increase the specific surface area of nitrate.

Physical properties of nanofluids

Adding nanoparticles into traditional heat transfer media thus forming nanofluids creates new type of enhanced heat transfer media. Song [25] prepared molten salt-based SiO_2 nanofluids by a melting-mechanical stirring method. The thermal stability of nanofluids is verified by maintaining a certain high-temperature and large temperature difference for the quenching cool and heat tests. The specific parameters of nanofluids, i.e., viscosity, thermal conductivity, specific heat and density, can be estimated as follows [28].

(1) Density, kg m^{-3}

The density ρ_{nf} of the nanofluids can be estimated as follows.

$$\rho_{nf} = 2043.9 - 0.5626 \times (T - 273.15) \quad 410\,K \le T \le 773\,K \tag{11}$$

(2) Specific heat, J kg^{-1} K^{-1}

The specific heat $(C_p)_{nf}$ can be estimated as follows.

$$\left(C_p\right)_{nf} = 1622.57 + 7.827 \times 10^{-4} \times (T - 273.15) \quad 410\,K \le T \le 773\,K \tag{12}$$

(3) Viscosity, Pa s

The viscosity of the nanofluids in the temperature range of 410–773 K can be expressed as follows.

$$\mu_{nf} = 9.28 \times 10^{-3} - 4.79 \times 10^{-5} \times (T - 273.15) + 7.30 \times 10^{-8} \times (T - 273.15)^2 \tag{13}$$

(4) Thermal conductivity, W m^{-1} K^{-1}

The thermal conductivity λ_{nf} can be estimated as follows.

$$\lambda_{nf} = 0.573 + 8.08 \times 10^{-4} \times (T - 273.15) \quad 410\,K \le T \le 773\,K \tag{14}$$

Result analysis

The distribution of velocity along with temperature for free convection heat transfer

Figure 6 exhibits temperature distributions for the molten salt with a temperature of 390 K on the top wall and temperatures of 450 K and 523 K on the bottom wall. Figure 7 gives temperature distributions for nanofluids during natural convection heat transfer at these temperatures. Figure 8 shows velocity distributions for the fusional salt with a temperature of 390 K on the top wall and temperatures of 450 K and 523 K on the bottom wall of the cylindrical cavity during free convection. Figure 9 gives the velocity distributions of nanofluids during natural convection heat transfer at these temperatures.

As illustrated in Fig. 6, during the molten salt free convection, there is significant thermal stratification in the cavity at the top and bottom with high temperature gradients. Nevertheless, the stratification is not pronounced in the middle section of the cavity. When the temperature of the bottom wall is high ($T = 523$ K), thermal stratification at the bottom is quite strong, and the heat is moving fast upward with pronounced temperature variations. On the other hand, when the temperature of the bottom wall is low ($T = 450$ K), heat moves up slowly with weaker temperature variations. Combining Figs. 6 and 8, one finds that the fluid flow at the bottom is relatively slow ($v_f = 0.0015$ m s^{-1}) at a lower bottom temperature of 450 K and heat transfer at the bottom wall is mild. At 523 K temperature at the bottom, the fluid flow is relatively fast ($v_f = 0.0023$ m s^{-1}) and heat transfer is strong.

In Fig. 7, the temperature distribution of nanofluids during free convection is very similar to that of molten salt. There is also a significant thermal stratification in the cavity at the top and bottom with high temperature gradients, and

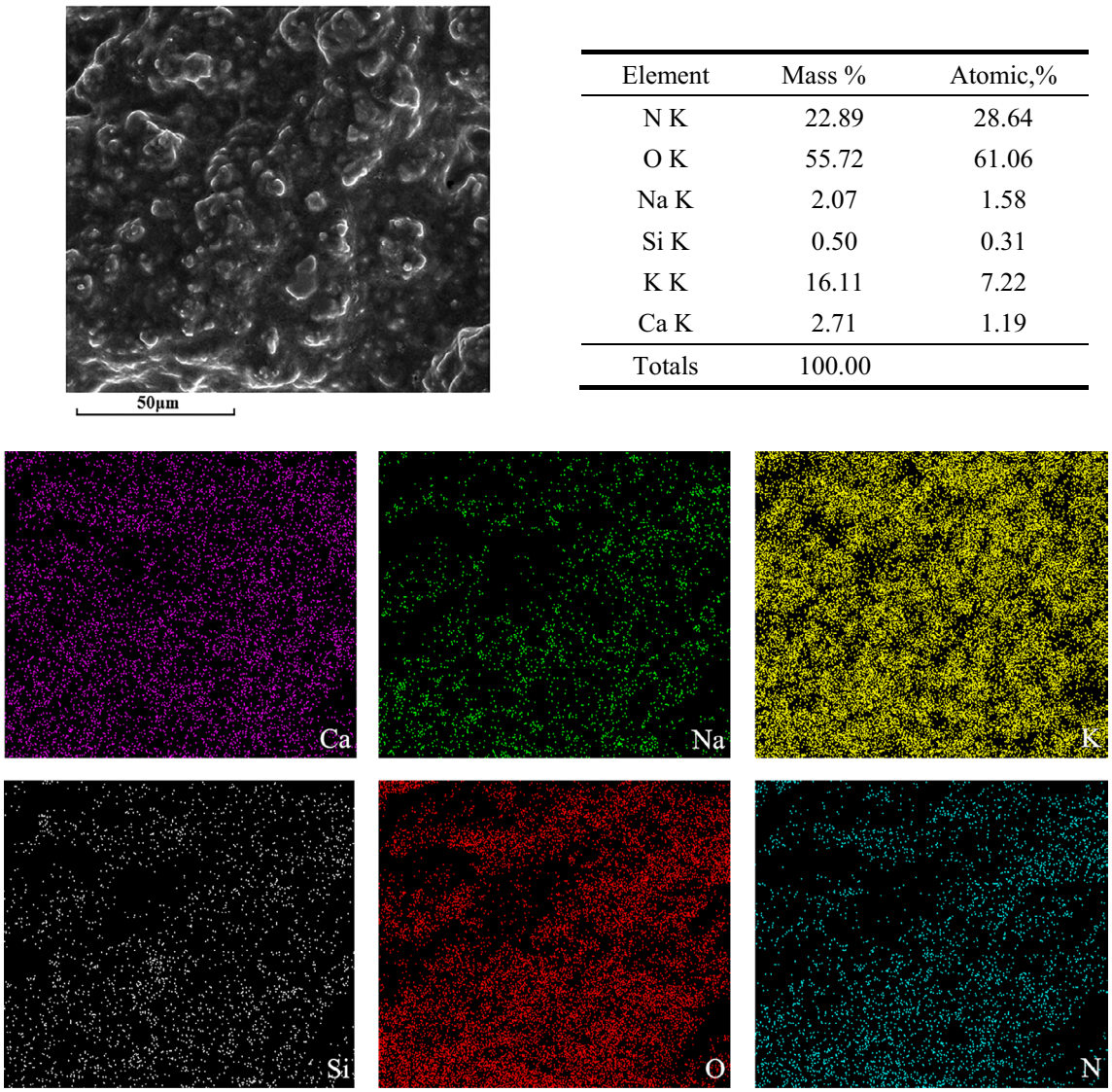

Element	Mass %	Atomic,%
N K	22.89	28.64
O K	55.72	61.06
Na K	2.07	1.58
Si K	0.50	0.31
K K	16.11	7.22
Ca K	2.71	1.19
Totals	100.00	

Fig. 5 EDS element mapping images of the molten salt nanocomposites

the stratification is not pronounced in the middle section. When the temperature of the bottom wall is at 450 K, the temperature variations are quite gentle. As the bottom wall temperature is increased (at 523 K), there is strong temperature changes at the bottom wall. Combining Fig. 7 and Fig. 9, one finds that the fluid flow at the bottom is relatively slow ($v_{nf}=0.0032$ m s^{-1}) at the low temperature of 450 K, but the fluid flow is relatively fast ($v_{nf}=0.0051$ m s^{-1}) and the heat transfer at the bottom wall is strong at the high temperature of 523 K. Comparing Fig. 7 with Fig. 6, one finds that at the same bottom and top temperatures, the thermal boundary layer at the bottom wall of nanofluid is thinner, which indicates that the heat transfer performance of nanofluid is better than that of liquid molten salt and the free convection heat transfer is enhanced. It is speculated that the Brownian motion of nanoparticles promotes the fluid flow and enhances the natural convection heat transfer. Tzou [29] studied the heat transfer of nanofluids and believed that the Brownian motion of nanoparticles can promote the convective motion of fluids.

According to Fig. 8, the fusional salt temperature increased after receiving heat from the bottom wall is at higher temperature, and the buoyancy force moves the fluid upward along the side wall of the cylindrical cavity. When the fluid reaches the top wall, it transfers heat to that wall and becomes cooler. It then moves downward from the middle section of the cylindrical cavity. When the temperature of the bottom wall is high ($T=523$ K), the fluid moves faster and creates great impact on the bottom wall. Heat transfer is also strong, and temperature stratification is significant making the thermal boundary layer thinner compared with the low temperature of 450 K. When the flow reaches a steady

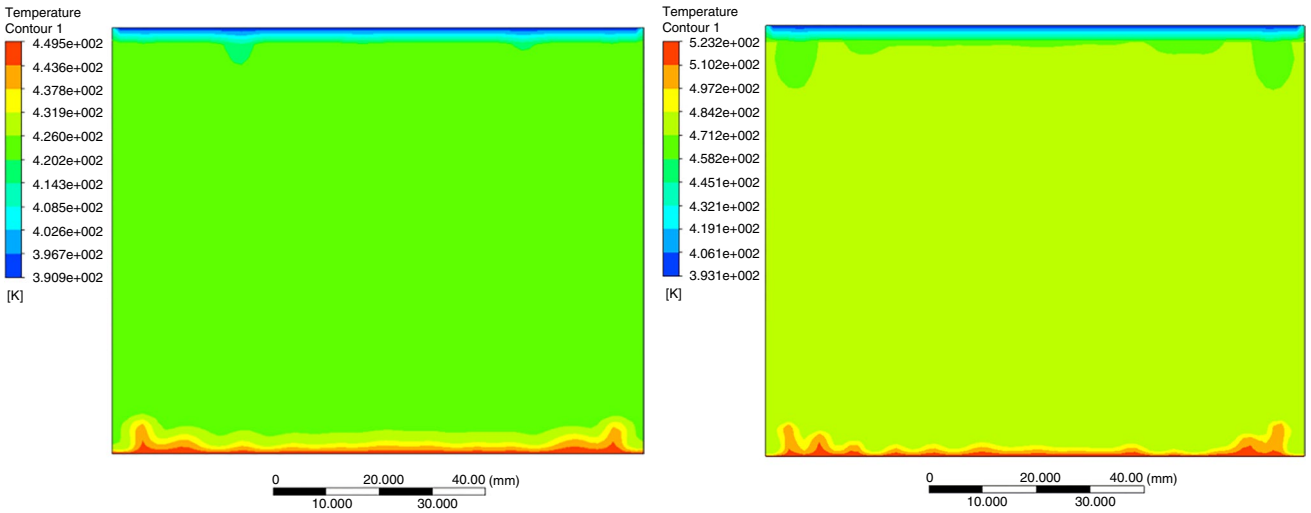

(a) Bottom temperature is 450 K **(b)** Bottom temperature is 523 K

Fig. 6 Temperature distributions of molten salt

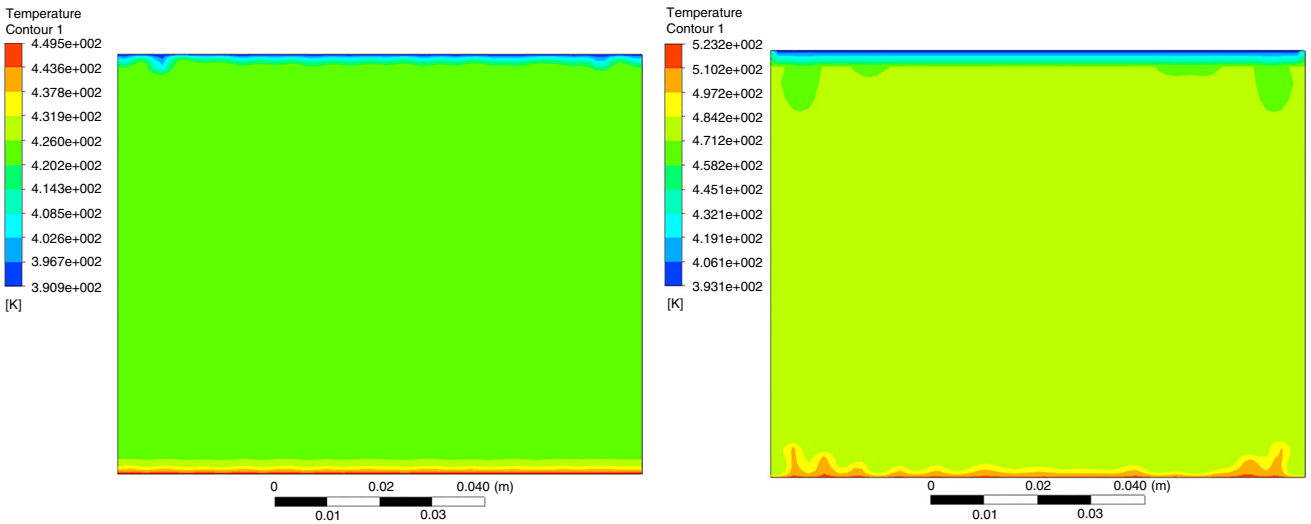

(a) Bottom temperature is 450 K **(b)** Bottom temperature is 523 K

Fig. 7 Temperature distributions of nanofluids

state, there are two symmetric vortices. Independent vortices are quite a few around the bottom wall at a low temperature of 450 K, while their appearance gradually increased as the temperature increases to 523 K. This was because a higher temperature of the bottom wall led to a more rapid heat transfer between the wall and fluid. Small localized vortices are formed by cool fluid elements flowing from the wall of a low temperature and hot fluid elements from the wall of high temperature. It is also indicated that the temperature variations are relatively stronger when the temperature of the bottom wall is higher.

From Fig. 9, the velocity distributions of nanofluids during natural convection heat transfer resemble the fusional salt velocity distributions. However, the free convection flow velocity of nanofluids ($v_{nf}=0.0051$ m s^{-1}) is higher than the velocity of the fusional salt ($v_f=0.0023$ m s^{-1}) at the same temperature of 523 K. It is inferred that the Brownian motion of the nanoparticles added to the fusional salt lowered the viscosity of the molten salt. (At 473 K, the dynamic viscosity of the nanofluids was 0.00262 Pa s, while that of molten salt was 0.004248 Pa s.) Therefore, it increases the instability of nanofluids flow and enhances the free convection

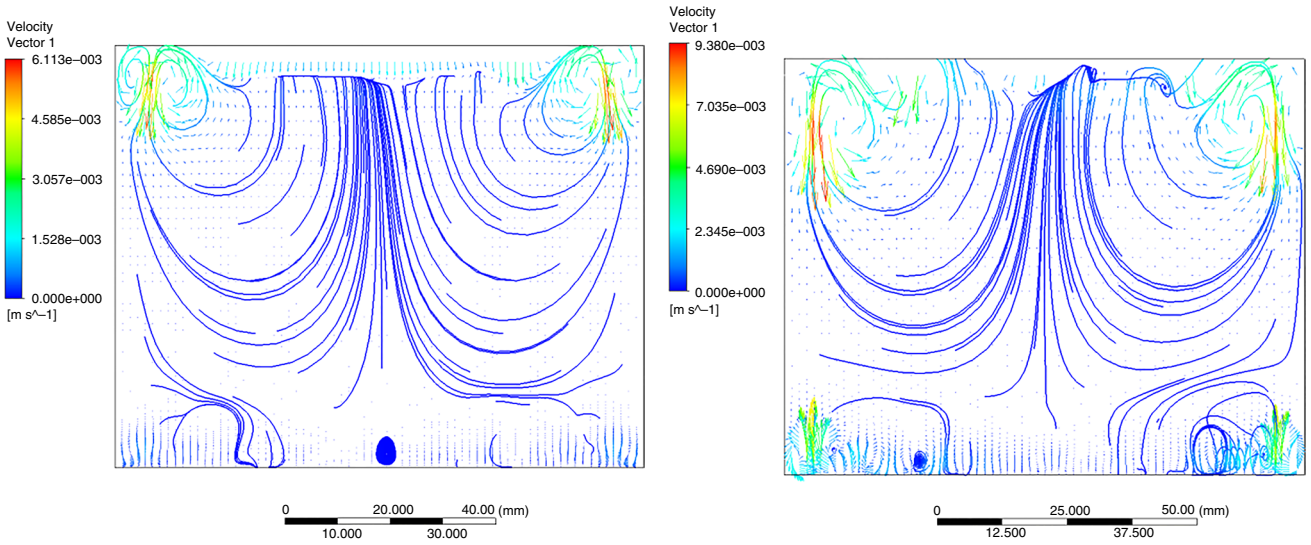

(a) Bottom temperature is 450 K **(b)** Bottom temperature is 523 K

Fig. 8 Velocity distributions of molten salt

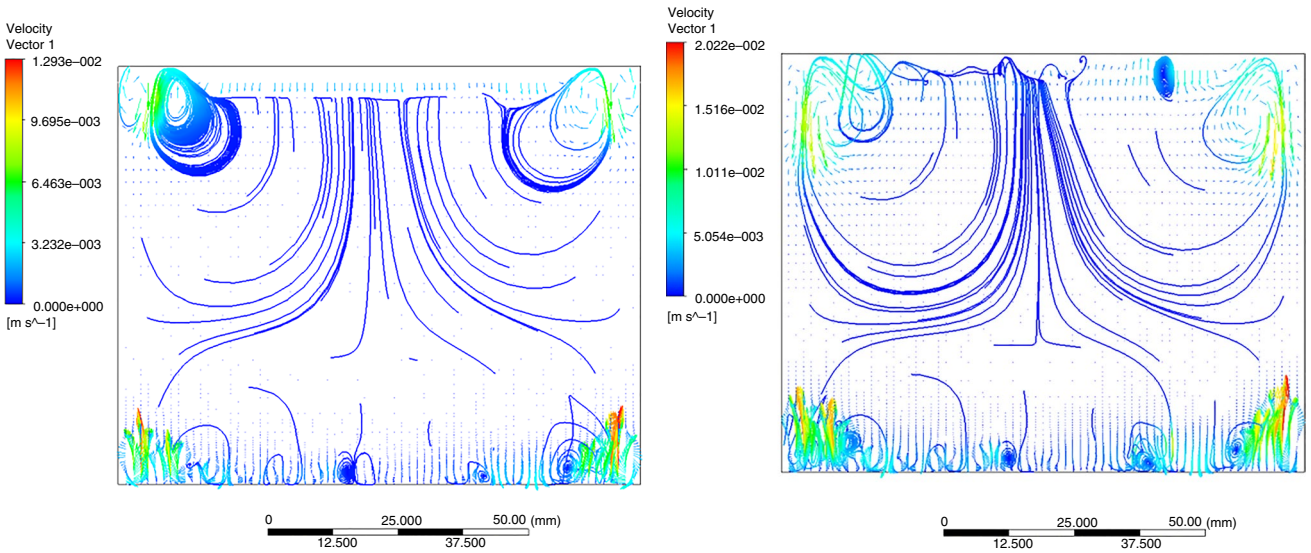

(a) Bottom temperature is 450 K **(b)** Bottom temperature is 523 K

Fig. 9 Velocity distributions of nanofluids

heat transfer of nanofluids. Ghasemi [30] also considered the influence of Brownian motion when studying natural convection heat transfer in a triangular enclosure filled with nanofluids.

Natural convection heat transfer law of molten salt nanofluids in a cylindrical cavity

Figure 10 shows experimental and simulated Nu numbers versus the Ra number of nanofluids, and comparisons with those of molten salt and water are provided. After addition of nanoparticles into the molten salt, the fluid free convection heat transfer is improved. The Nu number variation versus the Ra number of the nanofluids is consistent with that of the molten salt. This is because the dynamic viscosity of nanofluids (at 473 K, $\mu_{nf}=0.00262$ Pa s) is far smaller than that of molten salt (at 473 K, $\mu_f=0.004248$ Pa s). Thus, the velocity of the former is higher, leading to stronger natural convection heat transfer.

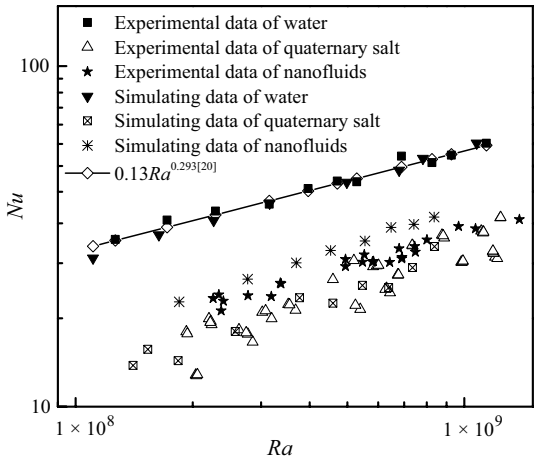

Fig. 10 *Nu* of nanofluids versus with *Ra*

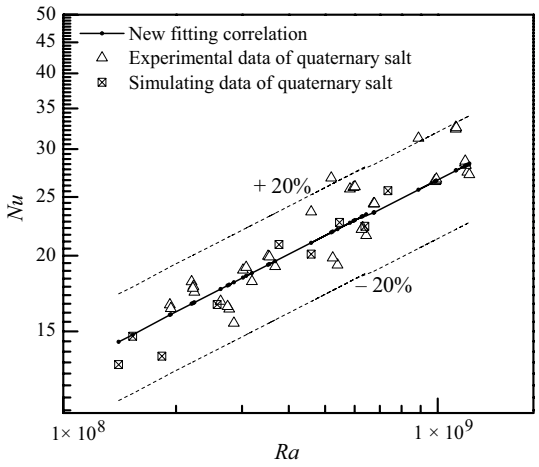

Fig. 12 Heat transfer correlation of molten salt

Putra [14] carried out experiments to study natural convection of Al_2O_3 based on water along with CuO nanofluids and found that the aggregation and sedimentation of nanoparticles worsened the natural convection heat transfer. This was because the densities of Al_2O_3 ($\rho = 3.7$ g cm^{-3}) and CuO ($\rho = 6.6$ g cm^{-3}) were significantly different from that of water ($\rho = 1$ g cm^{-3}), incurring their aggregation and sedimentation. In contrast, as SiO_2 ($\rho = 2.2$ g cm^{-3}) has approximately the same density as molten salt ($\rho_f = 2.04$ g cm^{-3}), it will not easily settle down. This is a principle reason why enhancement occurs of nanofluids of fusional salt convective heat transfer.

Figure 11 shows results of experiments and simulations for nanofluids free convection heat transfer compared with classical correlations. From Fig. 11, the Nu numbers from various classical correlations [31–34] of free convection

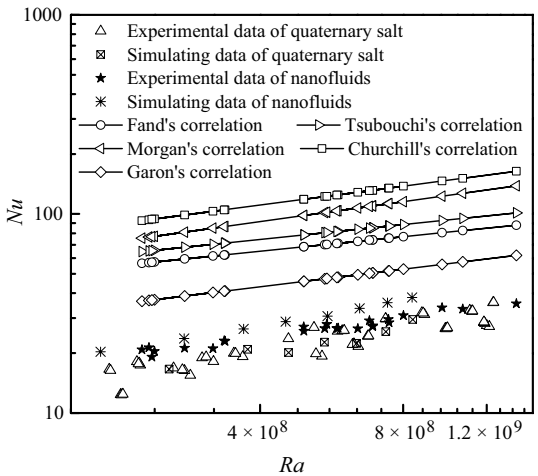

Fig. 11 *Nu* of nanofluids versus *Ra* and comparisons with other correlations

were quite different from the nanofluids Nu number. The predictions by Garon's correlation were closer to nanofluids free convection, followed by Fand's correlation. Fand's correlation could accurately predict fusional salt free convection on the surface of horizontal microcolumns [35, 36]. However, it cannot predict nanofluids free convection in the cylindrical cavity accurately. It is found that the nanofluids free convection heat transfer is better than that of molten salt after adding nanoparticles.

The *Nu* number of free convection in the cylindrical cavity is related to the *Ra* number. The relationship between *Nu* number and *Ra* number for natural convection of fusional salt was predicted within this paper. It was discovered that the free convection *Nu* number in pure fusional salts can be predicted by formula (15), and the results are revealed in Fig. 12.

$$Nu = 0.0445 \times \mathrm{Ra}^{0.308} \tag{15}$$

The maximum deviation of the experimental *Nu* and the fitting correlation was less than 20% between *Ra* 7×10^7 and 1.2×10^9. Moreover, the correlation could better predict the simulated results, and the error was within 10%. This is so as the vertical wall was insulated in the numerical calculations, which effectively reduced the influence of the heat loss and makes the calculation results closer to the predicted values. Therefore, free convection Nu number for fusional salt can be calculated by formula (15).

Nanofluids free convection Nu number can be calculated by formula (16). The results are revealed in Fig. 13.

$$Nu = 0.044 \times \mathrm{Ra}^{0.319} \tag{16}$$

The maximum deviation of the *Nu* number of simulations and fitting correlation as well as experiments was less than 20% between *Ra* 2×10^8 and 1.5×10^9. Hence, the free

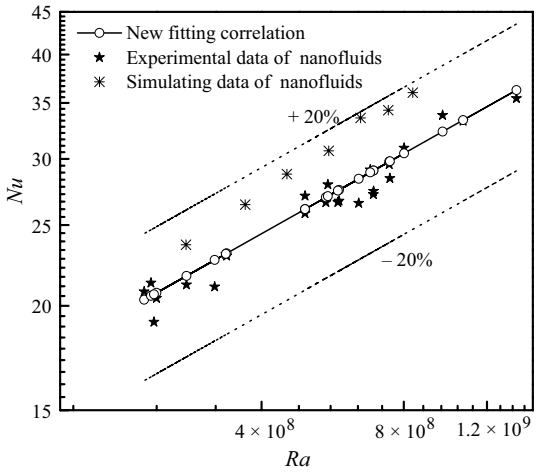

Fig. 13 Heat transfer correlation of nanofluids

convection Nu number of nanofluids can be calculated via formula (16).

Conclusions

Free convection heat transfer for molten salt nanofluids in a cylindrical cavity is studied using eutectic nitrate as the foundation salt and SiO_2 nanoparticles as additives. The results of experiments and numerical simulations reveal that:

1. The free convection heat transfer of nanofluids in the cylindrical cavity is similar to that of molten salt. The temperature gradient is large in the cylindrical cavity at the bottom and top wall, while the temperature in the cylindrical cavity middle is almost unchanged.
2. With the addition of nanoparticles (1 mass%), the viscosity of the nanofluids for molten salt is reduced, while the rate of flow is enhanced, which enhances the natural convection.
3. Density of SiO_2 nanoparticles is close to that of molten salts, which is liable to form stable molten slat nanofluids and enhance its heat transfer.
4. A new correlation between *Nu* number and *Ra* number is proposed. The correlation can predict nanofluids free convection accurately. The largest deviation of the correlation is below 20%, which is verified by both experimental data and simulation data.

Acknowledgements This work was supported by the National Natural Science Foundation of China with Grant Number 51576006, the Qinghai Science and Technology Project with grant number 2017-GX-A3 and National Key Research and Development Program of China with Grant Number 2017YFB0903603.

References

1. Duraisamy RR, Esakkimuthu GS, Paulraj J, et al. Review on influencing parameters in the performance of concentrated solar power collector based on materials, heat transfer fluids and design. J Therm Anal Calorim. 2019. https://doi.org/10.1007/s10973-019-08759-8.
2. Srivastva U, Malhotra RK, Kaushik SC. Review of heat transport properties of solar heat transfer fluids. J Therm Anal Calorim. 2017;130:605–21.
3. Zhang ZL, Yuan YP, Ouyang LP, et al. Enhanced thermal properties of Li_2CO_3-Na_2CO_3-K_2CO_3 nanofluids with nanoalumina for heat transfer in high-temperature CSP systems. J Therm Anal Calorim. 2017;128:1783–92.
4. Cui XM, Lu YW, Wu YT, et al. Influence of thermal stratification on discharging process of molten salt in single thermal storage tank. J Chem Ind Eng. 2018;69(6):2410–6 **(in Chinese)**.
5. Ahmed SE, Mansour MA, Hussein AK, et al. MHD mixed convection in an inclined cavity containing adiabatic obstacle and filled with Cu-water nanofluid in the presence of the heat generation and partial slip. J Therm Anal Calorim. 2019;138:1443–60.
6. Shirazi M, Shateri A, Bayareh M. Numerical investigation of mixed convection heat transfer of a nanofluid in a circular enclosure with a rotating inner cylinder. J Therm Anal Calorim. 2018;133:1061–73.
7. Rashmi W, Khalid M, Faridah Y. CFD studies on natural convection heat transfer of AlO-water nanofluids. Heat Mass Transf. 2011;47(10):1301–10.
8. Oztop HF, Abu-Nada E, Varol Y, et al. Computational analysis of non-isothermal temperature distribution on natural convection in nanofluid filled enclosures. Superlattices Microstruct. 2011;49(4):453–67.
9. Mahmoodi M. Numerical simulation of free convection of nanofluid in a square cavity with an inside heater. Int J Therm Sci. 2011;50(11):2161–75.
10. Lai FH, Yang YT. Lattice Boltzmann simulation of natural convection heat transfer of AlO/water nanofluids in a square enclosure. Int J Therm Sci. 2011;50(10):1930–41.
11. Sokhansefat T, Kasaeian AB, Kowsary F. Heat transfer enhancement in parabolic trough collector tube using Al_2O_3/synthetic oil nanofluid. Renew Sustain Energy Rev. 2014;33(2):636–44.
12. Mwesigye A, Huan Z, Meyer JP. Thermodynamic optimisation of the performance of a parabolic trough receiver using synthetic oil–Al_2O_3 nanofluid. Appl Energy. 2015;156:398–412.
13. Mwesigye A, Huan Z, Meyer JP. Thermal performance and entropy generation analysis of a high concentration ratio parabolic trough solar collector with Cu-Therminol®;VP-1 nanofluid. Energy Convers Manag. 2016;120:449–65.
14. Putra N, Roetzel W, Das SK. Natural convection of nano-fluids. Heat Mass Transf. 2003;39(8–9):775–84.
15. Suhaib UI, Rajashekhar P, Marneni N. Experimental investigation of natural convection heat transfer characteristics in MWCNT-thermal oil nanofluid. J Therm Anal Calorim. 2019;135:1197–209.
16. Subramanian R, Kumar AS, Vinayagar K, et al. Experimental analyses on heat transfer performance of TiO_2-water nanofluid in double-pipe counter-flow heat exchanger for various flow regimes. J Therm Anal Calorim. 2019. https://doi.org/10.1007/s10973-019-08887-1.
17. Torki M, Etesami N. Experimental investigation of natural convection heat transfer of SiO_2/water nanofluid inside inclined enclosure. J Therm Anal Calorim. 2019. https://doi.org/10.1007/s10973-019-08445-9.
18. Ming XH, Pan C. Experimental investigation of heat transfer performance of molten HITEC salt flow with alumina nanoparticles. Int J Heat Mass Transf. 2017;107:1094–103.

19. Lu YW, Yu Q, Du WB, et al. Natural convection heat transfer of molten salt in a single energy storage tank. Sci China Technol Sci. 2016;59(8):1244–51.
20. Garon AM, Goldstein RJ. Velocity and heat transfer measurements in thermal convection. Phys Fluids. 1973;16(11):1818–25.
21. Ren N, Wu YT, Ma CF, et al. Preparation and thermal properties of quaternary mixed nitrate with low melting point. Sol Energy Mater Sol Cells. 2014;127(4):6–13.
22. Ren N, Wu YT, Ma CF. Experimental study of viscosity of new kind of molten salt with low melting point. J Eng Thermophys-Rus. 2012;33(3):497–500.
23. Chieruzzi M, Cerritelli GF, Miliozzi A, et al. Effect of nanoparticles on heat capacity of nanofluids based on molten salts as PCM for thermal energy storage. Nanoscale Res Lett. 2013;8(1):448.
24. Andreucabedo P, Mondragon R, Hernandez L, et al. Increment of specific heat capacity of solar salt with SiO_2 nanoparticles. Nanoscale Res Lett. 2014;9(1):582.
25. Song WL, Lu YW, Wu YT, et al. Effect of SiO_2 nanoparticles on specific heat capacity of low-melting-point eutectic quaternary nitrate salt. Sol Energy Mater Sol Cells. 2018;179:66–71.
26. Shin D, Banerjee D. Enhanced thermal properties of SiO_2 nanocomposite for solar thermal energy storage applications. Int J Heat Mass Transf. 2015;84:898–902.
27. Zhang LD, Chen X, Wu YT, et al. Effect of nanoparticle dispersion on enhancing the specific heat capacity of quaternary nitrate for solar thermal energy storage application. Sol Energy Mater Sol Cells. 2016;157:808–13.
28. Song WL. Preparation and thermal physical properties analysis of molten-salt nanocomposites. Beijing: Beijing University of Technology; 2018.
29. Tzou DY. Thermal instability of nanofluids in natural convection. Int J Heat Mass Transf. 2008;51(11–12):2967–79.
30. Ghasemi B, Aminossadati SM. Brownian motion of nanoparticles in a triangular enclosure with natural convection. Int J Therm Sci. 2010;49(6):931–40.
31. Churchill SW, Chu HHS. Correlating equations for laminar and turbulent free convection from a horizontal cylinder. Int J Heat Mass Transf. 1975;18(9):1049–53.
32. Fand RM, Brucker J. A correlation for heat transfer by natural convection from horizontal cylinders that accounts for viscous dissipation. Int J Heat Mass Transf. 1983;26(5):709–16.
33. Morgan VT. The overall convective heat transfer from smooth circular cylinders. Adv Heat Transf. 1975;11:199–264.
34. Tsubouchi T, Masuda H. Natural convection between horizontal concentric cylinders with density inversion of water for low Rayleigh numbers. Rep Inst High Speed Mech Jpn. 1967;190(19):205–19.
35. Lu YW, Li XL, Li Q, et al. Numerical simulation and experimental investigation of natural convection heat transfer of molten salt around fine wire. Sci China Technol Sci. 2013;56(7):1651–6.
36. Lu YW, Li XL, Du WB, et al. Natural convection heat transfer of molten nitrate around horizontal cylinder. J Chem Ind Eng. 2015;66(3):949–54 **(in Chinese)**.